Nanoscale

Solid-state electrochemical oxidation with polyelectrolyte membrane stamps for micro-/nanoscale pattern formation on Au surfaces

Journal:	*Nanoscale*
Manuscript ID	NR-ART-07-2024-002978.R1
Article Type:	Paper
Date Submitted by the Author:	20-Sep-2024
Complete List of Authors:	Fujii, Tatsuya; Ritsumeikan Daigaku, Department of Mechanical Engineering Tsuji, ATSUKI; Ritsumeikan Daigaku, Department of Mechanical Engineering Takizawa, Masaru; Ritsumeikan Daigaku Rikogakubu Daigakuin Rikogaku Kenkyuka Murata, Junji; Ritsumeikan Daigaku, Department of Mechanical Engineering

SCHOLARONE™
Manuscripts

Please do not adjust margins

ARTICLE

Solid-state electrochemical oxidation with polyelectrolyte membrane stamps for micro-/nanoscale pattern formation on Au surfaces

Received 00th January 20xx,
Accepted 00th January 20xx

DOI: 10.1039/x0xx00000x

Tatsuya Fujii[a], Atsuki Tsuji[a], Masaru Takizawa[b] and Junji Murata[a,*]

Nanoscale-patterned Au surfaces are promising for a wide range of applications from bio/chemical sensors to high-performance electrodes. However, pattern formation using conventional resist-based methods is complex, expensive, and environmentally unfriendly. Herein, we report a novel approach for pattern formation on Au surfaces using solid-state electrochemical treatment with polymer electrolyte membrane (PEM) stamps. During electrolysis, the patterned structure of the PEM stamp was transferred onto the Au surface to form micro- and nanoscale oxide patterns. X-ray analysis of the treated surface confirmed the formation of an oxide film on the Au surface, which was subsequently reduced to metallic Au after air exposure for several weeks. Although the pattern height decreased with air exposure, a patterned structure with a height of several hundred nanometers was maintained following oxide reduction. Reflectance spectroscopy revealed that the patterned Au surface exhibited sharp reflectance peaks, the intensities and positions of which strongly depended on the measurement angle, which are key characteristics of diffraction gratings. This fast and facile electrochemical treatment process is promising for the preparation of patterned Au surfaces that can be applied in optical gratings and localized surface plasmon resonance sensors.

1. Introduction

Noble metals, including Pt, Pd, and Au, which exhibit extremely high chemical inertness and high catalytic activity, have been used in various applications such as catalysts for chemical synthesis[1], electrodes for fuel cells[2], and biochemical[3] or chemical sensors[4]. Based on the localized surface plasmon resonance (LSPR) characteristics of nanoscale Au materials, surface-enhanced Raman spectroscopy has become a well-known technique for ultrasensitive sensing[5]. Furthermore, Au-based LSPR templates with patterned structures have been applied in sensors to detect biomolecules and toxic gases. For example, Monkawa et al.[6,7] demonstrated that a nanopatterned Au surface with a porous silica layer can be employed as an effective and highly sensitive LSPR sensor for harmful gases such as volatile organic compounds and SO_2. However, Au-based LSPR tips are typically prepared using photolithographic techniques[8], which involve numerous complex processes, including resist coating, electron beam exposure, development, dry etching, and residual photoresist removal. Along with extremely expensive facilities, the use of photoresists requires high-temperature annealing and generates large amounts of waste liquid that must be treated. Consequently, this approach is energy-intensive and costly with a significant environmental impact. Energy beam-assisted processing such as focused ion beam[9] and laser beam machining can be used to form patterned structures on highly stable materials. However, generating the energy beam requires significant energy consumption. Furthermore, as reported by Do et al.[10], the resolution of direct laser beam machining is limited to hundreds of micrometres. Submicrometric patterning on Au films can only be achieved via an indirect method involving the use of a resist[11].

The nanoimprint lithography (NIL) technique, first introduced by Chou et al.[12] in 1996, is a promising patterning process because of its simple pattern-formation mechanism based on the plastic deformation of materials. In thermal NIL, patterns are directly transferred from a master mold surface onto soft polymer materials by pressing the mold onto the material surface under high-temperature conditions. However, direct processing is limited to polymeric materials. As forming patterns directly on hard materials such as metals and semiconductors is difficult, a resist film produced by NIL on the material surface is instead employed as an etching or deposition mask[13]. This multistep process eliminates the main advantages of NIL, namely, direct processing and simplicity. The direct formation of patterns on metal surfaces without employing a resist film has been demonstrated using extremely high-pressure NIL[14]. However, the application of high pressure can shorten the lifespan of the master mold and damage the material surface via plastic deformation.

Methods for preparing patterned Au surfaces based on nanoparticle manipulation have attracted considerable attention. Au nanoparticle arrays[15,16], in which particles are aligned on

[a] Department of Mechanical Engineering, Ritsumeikan University, Kusatsu, Shiga, Japan
E-mail: murata-j@fc.ritsumei.ac.jp
[b] Department of Physical Sciences, Ritsumeikan University, Kusatsu, Shiga, Japan

Please do not adjust margins

patterned templates, have been proposed for use in LSPR sensors. Disadvantageously, the procedures for preparing patterned templates, such as anodic porous alumina substrates, are complex and nanoparticle arrays exhibit poor durability against friction because the Au nanoparticles are readily detached from the sample surface. In colloidal lithography techniques[17,18], a particle monolayer regularly arranged on a flat substrate is employed as a mask for Au thin-film deposition. However, the generation of a particle array at a liquid–water interface generally introduces defects and disordered grains, which can affect the optical properties of LSPR tips.

Although wet chemical etching is a damage-free process, the high chemical inertness of noble metals requires extremely acidic etchants. Only aqua regia, a mixed aqueous solution of concentrated nitric and hydrochloric acids, can etch Au surfaces[19]. As an alternative to acid–base wet etching, Nishio et al.[20,21] oxidized Au surfaces via an electrochemical surface modification technique using a milder carboxylic acid to form nanoporous structures on the treated Au surface. However, uniform contact between the anode surface and electrolyte induces uniform oxidation of the Au surface, which complicates direct pattern formation via this method. Furthermore, the use of large amounts of harsh chemicals as liquid electrolytes necessitates liquid waste treatment, resulting in a high environmental burden.

We previously reported a novel electrochemical surface treatment method that does not require liquid electrolytes[22–28]. Specifically, replacing the liquid electrolyte with a polymer electrolyte membrane (PEM) enables solid-state electrochemical surface processing. Using this approach, the highly efficient room-temperature electrochemical oxidation of Si[22,28], Ti[24], GaN[27], and SiC[23,25] has been achieved without the use of harsh liquid chemicals. After discovering anodic dissolution at the interface between the PEM and a Cu surface, this phenomenon was successfully exploited for the direct nanoscale patterning of Cu[26]. This method is suitable for the rapid modification and etching of metal and semiconductor surfaces at the micro- and nanoscale. As no resist films, liquid chemicals, or high-temperature treatments are required, this simple and direct pattern formation technique offers significant advantages in terms of processing and environmental costs. However, the treatment of noble metals, such as Au and Pt, using PEM-based solid-state electrochemistry has not yet been reported. In this study, we investigated the interfacial chemical reaction between PEM and Au surfaces and its application to microscale pattern formation. In addition to electrochemical measurements, the chemical states of Au surfaces modified via solid-state electrolysis were analysed using synchrotron radiation X-ray and electron microscopy techniques. The structures and morphologies of the microscale patterns formed using PEM stamps with patterned surfaces were evaluated using scanning probe microscopy. Furthermore, time-dependent changes in the chemical states, optical properties, and structures of the patterns formed on the Au surface were investigated.

2. Experimental

A commercially available short-side-chain perfluorosulfonic acid (PFSA; $CF(CF_2)_n$–O–$(CF_2)_2$–SO_3H) ionomer membrane[29] with a thickness of 90 µm (Aquivion, E98-09S, Solvay) was employed as the PEM for solid-state electrolysis. The polymer-based solid electrolyte has soft and flexible characteristics compared to superionic conductors[30], which have been used for electrochemical nanofabrication, making it suitable for the facile preparation of stamps with micro- and nanoscale pattern structures. Furthermore, unlike other solid electrolytes, PEM exhibits high ion conductivity at room temperature[31], enabling the electrochemical patterning process to operate at low temperature. As shown in Fig. 1(a), PEM stamps were prepared via a hot embossing process, in which the patterned structure of a master mold (DTM2-2, Kyodo International Inc.) was transferred onto the PEM surface by plastic deformation of the membrane. The pristine PEM was pressed onto the master mold at a pressure of 5 MPa and temperature of 135 °C for 6 min. After cooling to room temperature (~22 °C), the PEM was detached from the master mold to obtain a PEM stamp. The surface morphology of the prepared PEM stamp was observed using optical microscopy (OM; BX53MRF-S, Olympus) and atomic force microscopy (AFM; SPM-9700HT, Shimadzu Corp.).

The material used in this study was a sputtered Au thin film

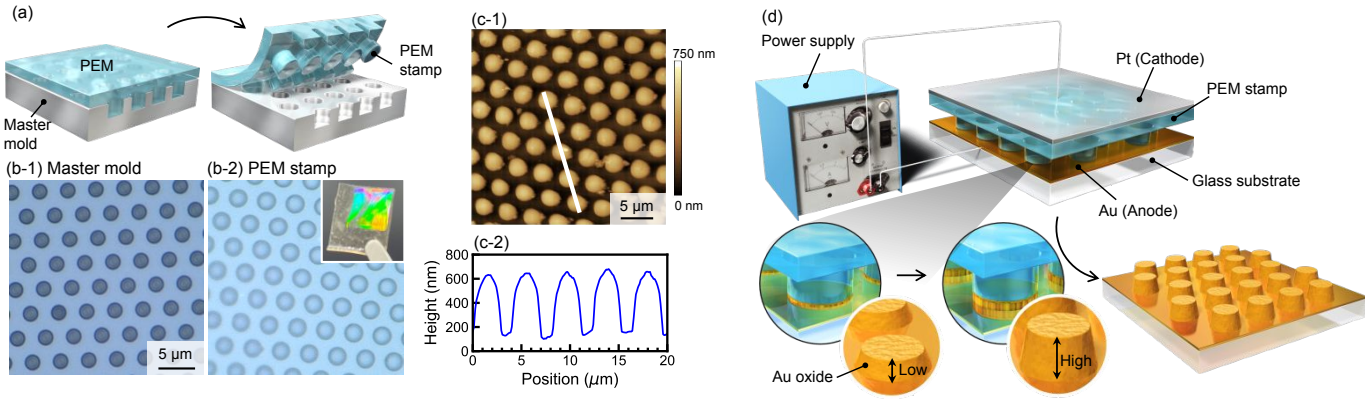

Fig. 1 (a) Schematic illustration of the hot embossing process used to prepare the PEM stamp. (b) OM images of (b-1) master mold and (b-2) PEM stamp surfaces. The inset in (b-2) shows a photograph of the PEM stamp. (c-1) AFM image of the PEM stamp with a 2 µm hcp columnar structure and (c-2) cross-sectional profile along the line in (c-1). (d) Schematic illustration of the solid-state electrochemical oxidation of a Au surface with the PEM stamp.

This journal is © The Royal Society of Chemistry 20xx

with a thickness of approximately 220 nm deposited on an 80 µm thick quartz template. An ultrathin Cr interlayer (~7 nm) was applied between the Au film and substrate to increase the adhesion of the Au film[32]. Although the Cr interlayer is believed not to affect the electrochemical reaction between the Au surface and the PEM stamp, it is essential for preventing the delamination of the Au film from the substrate during the electrochemical process.

Cyclic voltammetry (CV) and linear sweep voltammetry (LSV) were performed on a Au anode/PEM/Pt cathode electrochemical cell using an electrochemical measurement system (potentiostat/galvanostat, HZ-7000, Hokuto Denko Corp.). A nonpatterned flat PEM was employed for electrochemical measurements without a liquid electrolyte. The potential of the working electrode (Au) was controlled against that of the counter electrode (Pt), and no reference electrode was employed. During measurements, a constant pressure of 1.52 MPa was applied to the electrodes at a constant temperature of ~25 °C and relative humidity of 60%.

To analyse the chemical states of the Au surfaces treated using solid-state electrolysis, X-ray photoelectron spectroscopy (XPS) measurements were performed at BL-7 of the Synchrotron Radiation (SR) Center, Ritsumeikan University, with an Al *K*α X-ray source under an ultrahigh vacuum of ~7×10^{-8} Pa at room temperature (~22 °C). X-ray absorption spectroscopy (XAS) analysis was conducted at BL-13 of the SR Center under an ultrahigh vacuum of ~10^{-7} Pa at room temperature. X-ray absorption fine structure (XAFS) spectra were obtained using the total electron yield (TEY) at an evaluation depth of ~50 nm. To prepare the samples for XPS and XAFS analyses, a nonpatterned PEM was employed during electrolysis. Time-dependent changes in the chemical states were monitored by performing X-ray analyses on the treated Au samples after air exposure for 1, 2, and 12 weeks.

Patterning of the Au surfaces using the prepared PEM stamps was conducted using an apparatus specifically designed for solid-state electrolysis, as illustrated in Fig. 1(d). All other conditions, such as pressure and the surrounding atmosphere, were the same as those used for the above-described CV and LSV measurements. To achieve uniform contact between the PEM stamp and the Ag anode, a rubber membrane sheet was placed and pressed on the Pt cathode (a thin foil with a thickness of 0.01 mm). The combination of the rubber membrane and the flexible PEM stamp prevented the glass substrate from breaking under the high contact pressure (1.52 MPa).

The impact of the water content of the PEM stamps (wet/dry PEM) on the pattern structure was investigated. The water PEM was prepared by immersion in deionized water, while the dry PEM was the as-fabricated PEM. After electrolysis, the treated Au surfaces were examined using OM, AFM, and scanning electron microscopy (SEM; SU6600, Hitachi High-Tech Corp.) with built-in energy-dispersive X-ray spectroscopy (EDX; INCA-X, Oxford Instruments). The reflectance spectra of the treated Au surfaces were collected using a halogen lamp (Luminar Ace LA-100USW, Hayashi-Repic Co. Ltd.) as the incident light source, which passed through a 50 µm slit, combined with an optical fibre spectrometer (PMA-12, Hamamatsu Photonics). The incident angle of the halogen lamp was fixed at 60°, and the light reflected on the material surface was analysed at different reflection angles θ. The contact angle (CA) of a water droplet (~2 µL) on the Au surfaces was measured using an automatic contact angle meter (Dropmaster DMC-MC3, Kyowa Interface Science Co., Ltd.).

3. Results and discussion

3.1 Preparation of PEM stamp

The OM image (Fig. 1(b-2)) and AFM image (Fig. 1(c-1)) of the prepared PEM stamp confirmed the successful transfer of a patterned structure with a hexagonal closed-packed (hcp) arrangement from the master mold (Fig. 1(b-1)). As shown in the inset of Fig. 1(b-2), the PEM stamp exhibited rainbow structural coloration, which is caused by light interference in the regularly arranged structure. The diameter of the bumps formed on the stamp was slightly larger than that of the master mold (2 µm). Specifically, the bumps had a full width at half maximum (FWHM) of approximately 2.5 µm with a width at the bottom of more than 3 µm, as confirmed by the cross-sectional profile obtained from the AFM image (Fig. 1(c-2)). This enlargement of the pattern diameter is believed to originate from volume expansion of the PEM caused by water swelling[33]. During the preparation process, water within the PEM was removed by evaporation because of the high temperature (~150 ºC) applied for thermal embossing. After being released from the master mold, the PEM stamps were cooled and exposed to air. After the thermal process, the dried PEM stamps were "thirsty" and thus

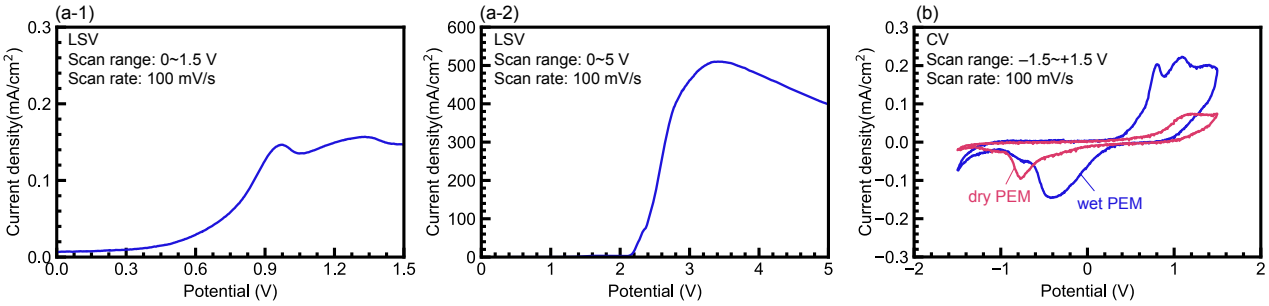

Fig. 2 Electrochemical measurements of the solid-state electrochemical oxidation process at the interface between PEM and Au surfaces. (a) LSV profiles at a scan rate of 10 mV/s in the scan ranges of (a-1) 0–1.5 V and (a-2) 0–5 V. (b) CV profiles with wet and dry PEM stamps.

immediately absorbed moisture from the surrounding atmosphere, resulting in swelling and thus increasing the dimensions of the formed pattern.

3.2 Electrochemical oxidation characteristics of Au surfaces

Electrochemical measurements were conducted using a nonpatterned PEM. The LSV profile obtained using the wet PEM at a scan rate of 100 mV/s in the scan range of 0–1.5 V (Fig. 2(a-1)) exhibited a peak at approximately 0.9 V. When a larger scan range (0–5 V) was used, a larger peak was observed at approximately 3 V, and the current density decreased at biases higher than 3 V. The CV profiles of the Au electrode (Fig. 2(b)) clearly indicate that the current density of the wet PEM was greater than that of the dry PEM, suggesting that the ion conductivity of the PEM strongly depends on its water content. Increased electrolytic current densities for wet PEMs were also observed in previous studies on the solid-state electrochemical oxidation and dissolution of Si[28] and Cu[26]. Ions such as protons (H^+) can be transferred between the electrodes via nanoscale water channels in the PEM formed by the hydrophilic sulfonic acid groups of PFSA. When the water content of the PEM is high, water channels are effectively generated, resulting in higher ion conductivity[34]. The anodic peaks observed in the potential range from 0.7 to 1.2 V were attributed to the surface oxidation of the Au anode. Multiple anodic peaks were only observed for the wet PEM, resulting from the oxidation of different surface orientations, as reported by Olaya et al[35]. In contrast, the profile for the dry PEM shows a single anodic peak. Since the electrochemical measurement was conducted without a reference electrode, the actual potential applied to the Au electrode for the dry PEM was lower due to a higher *IR* drop compared to the wet PEM. Consequently, a higher voltage is believed to be required to observe multiple anodic peaks in the dry PEM profile. The cathodic current peaks for both dry and wet PEMs can be attributed to the reduction of the oxidized surface. The peak shift toward higher negative potential for the dry PEM was also caused by the higher *IR* drop.

The chemical compositions of the Au surfaces treated with the nonpatterned PEM were analysed using XPS. As shown in Fig. 3(a), the XPS survey scans of the untreated surface and the surfaces treated with wet and dry PEMS all contained clear Au 4*f*, 4*d*, and 4*p* peaks, although the peak intensities differed significantly. A weak F 1*s* peak at a binding energy (BE) of approximately 690 eV was only observed for the treated

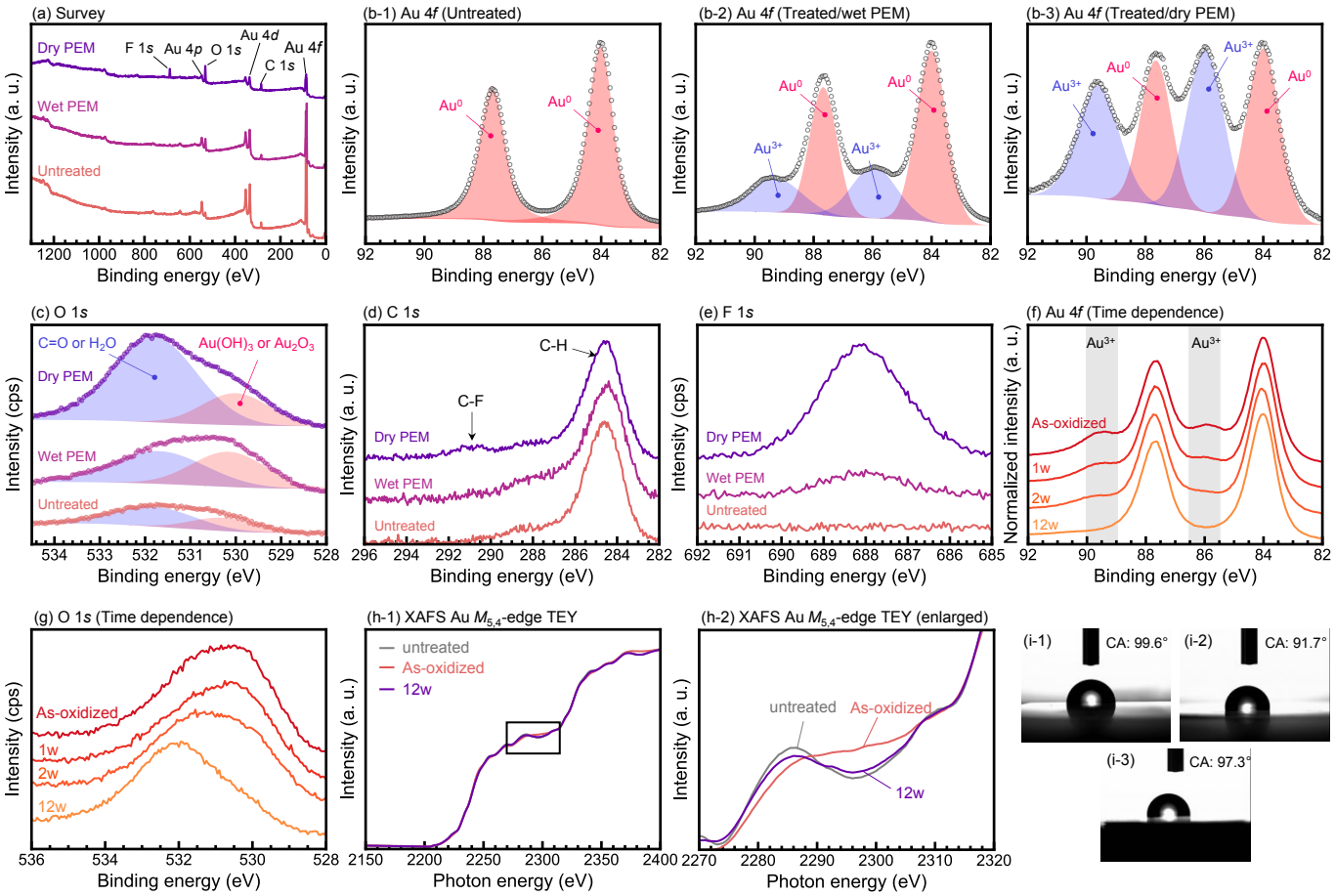

Fig. 3 Synchrotron radiation X-ray analysis of Au surfaces before and after solid-state electrochemical treatment using nonpatterned PEM. (a–g) XPS spectra: (a) survey scan; (b) Au 4*f* curve fitting for the (b-1) untreated surface, (b-2) surface treated using the wet PEM, and (b-3) surface treated using the dry PEM; (c) O 1*s*, (d) C 1*s*, and (e) F 1*s* core-level spectra for the untreated surface and wet/dry PEM-treated surfaces; (f) Au 4*f* and (g) O 1*s* spectra of the wet PEM-treated surface after air exposure at room temperature for 0, 1, 2, and 12 weeks. (h-1) Au $M_{5,4}$-edge XAFS TEY spectra of Au surfaces before and after solid-state electrolysis at evaluation depths of ~50 nm; (h-2) enlargement of (h-1). (i) Water CAs of Au surfaces: (i-1) untreated surface, (i-2) as-oxidized surface, and (i-3) oxidized surface after air exposure for 2 months.

This journal is © The Royal Society of Chemistry 20xx

surfaces. For the untreated surface, peak deconvolution of the Au 4*f* spectrum (Fig. 3(b-1)) revealed two components separated by a BE of 3.7 eV. These peaks derived from spin-orbit splitting were attributed to unoxidized metallic Au (i.e., Au^0 $4f_{7/2}$ and $4f_{5/2}$ at BEs of 83.9 and 87.5 eV, respectively)[20,21,36,37]. No clear satellite peaks were observed in this spectrum. In addition to the metallic Au^0 peaks, the Au 4*f* spectrum of the surface treated with the wet PEM (Fig. 3(b-2)) also contained two strong components at higher BEs, which were assigned to Au^{3+} $4f_{7/2}$ (85.9 eV) and $4f_{5/2}$ (89.5 eV)[20,21,36]. These results clearly demonstrate that gold oxide (Au_2O_3) or hydroxide ($Au(OH)_3$) can be formed on highly inert Au surfaces via solid-state electrochemical treatment at room temperature without any harsh chemicals. Furthermore, the intensities of the Au^{3+} oxide peaks were further increased in the Au 4*f* spectrum of the surface treated with the dry PEM (Fig. 3(b-3)), suggesting that electrochemical treatment using the dry PEM formed a thicker oxidized layer on the Au surface than that using the wet PEM, which will be discussed later.

Fig. 3(c) shows the O 1*s* spectra of the untreated and dry or wet PEM-treated surfaces. The deconvolution of the O 1*s* spectra shows that all tested Au surfaces have the same components at BEs of approximately 530 and 532 eV, although the intensities of each component differ between samples. The peak at 532 eV, which was the dominant component for the untreated surface, was attributed to water adsorbed on the surface[36] or organic contaminants (C=O)[37]. An additional peak at a lower BE of approximately 530 eV, which may originate from $Au(OH)_3$ and Au_2O_3[38], was clearly observed for the Au surfaces treated with both the dry and wet PEMs. Notably, the relative intensities of the O 1*s* peaks differ significantly for the surfaces treated with the dry and wet PEMs. Differences in the chemical states of metal surfaces treated with dry and wet PEMs were also observed in our previous study on Cu anodic etching using a PEM stamp[26]. In particular, Cu^{2+} oxidation peaks were observed for the surface treated with the dry PEM, whereas the Cu surface treated with the wet PEM consisted of metallic components. This behaviour can be attributed to dissolution of the oxide layer by a strongly acidic water layer at the interface between the wet PEM and material surface owing to the presence of sulfonic groups ($-SO_3H$) in the PEM. The lower Au^{3+} peak intensity for the wet PEM than that for the dry PEM is also believed to be due to the dissolution of the oxide film into the acidic water layer existing in the interface region between the wet PEM and the Au surface. However, unlike the electrochemical reaction of Cu, the oxide film was still formed on the Au surface even when the wet PEM was used for the electrolysis. The difference in the electrochemical reactions, namely anodic oxidation for the Au surface and dissolution for the Cu surface, can be explained using a pH-potential equilibrium diagram (Pourbaix diagram)[39]. According to the diagram, the Cu surface can dissolve into the electrolyte, generating Cu^{2+} ions under high potential and acidic conditions ($pH < 7$). In contrast, the diagram indicates that a much stronger acidic condition ($pH < 1$) is required to etch the Au surface, and $Au(OH)_3$ can form over a wide pH range from 1 to 12.

Fig. 3(f) shows the change in the Au 4*f* spectra upon exposure to air after electrochemical treatment using the wet PEM. The intensity of the Au^{3+} oxide peak gradually decreased as the duration of air exposure increased. Weak Au^{3+} peaks were still present after 2 weeks of air exposure, but these peaks disappeared after 12 weeks in an air atmosphere. Furthermore, as shown in Fig. 3(g), the O 1*s* peak shifted from a BE of ~530 eV (gold oxide or hydroxide) to ~532 eV (C=O) upon prolonged air exposure. These results clearly indicate that the gold oxide or hydroxide formed by the solid-state electrochemical treatment was gradually reduced to metallic Au via air exposure at room temperature. Nishio et al.[20] reported that a Au surface was oxidized by anodic oxidation in a carboxylic acid liquid electrolyte and that the resulting anodic gold oxide film re-formed the metallic state in an air owing to the noble nature of Au.

As shown in Fig. 3(d), hydrocarbon components originating from organic contamination were observed in the C 1*s* spectra of the surfaces treated with both the wet and dry PEMs. However, a weak peak at a BE of approximately 291 eV was observed for the surface treated with the dry PEM, whereas this peak was negligible for the surface treated with the wet PEM. The F 1*s* spectra of the surfaces treated with the dry and wet PEMs both exhibited a peak at a BE of 688 eV (Fig. 3(e)), although this peak was more intense for the surface treated with the dry PEM. In contrast, no peaks were observed in the F 1*s* spectrum of the untreated surface. As a clear F 1*s* peak was only observed for the treated surfaces, the weak peak in the C 1*s* spectrum of the surface treated with the dry PEM was assigned to a fluorocarbon (C–F) component derived from the main chain of PFSA. In our previous study, the PEM stamp was partially decomposed after electrolysis, and the highly oxidative species generated by electrolysis at the interface between the PEM and material surface could attack the PEM surface[26]. Such fluorocarbon contaminants were also observed in our previous study on Cu patterning via solid-state anodic etching when dry PEM stamps were applied[26], as confirmed by XPS and XAS. However, when a wet PEM was used for electrolysis, the thin water layer at the Au–PEM interface could act as a lubricant, hindering strong adhesion between the PEM and material surfaces. Consequently, lower C–F and F 1*s* peak intensities were observed for the surface treated with the wet PEM.

As depicted in the XAFS TEY spectra (Fig. 3(h-1)), no notable differences were observed between the untreated surface and the surface treated using the wet PEM. However, a magnified view of the spectra at a photon energy of ~2300 eV (Fig. 3(h-2)) revealed a clear difference between the samples before and after electrochemical oxidation. The untreated surface exhibited a peak and valley at photon energies of ~2286 and ~2296 eV, respectively. However, for the as-oxidized surface, an increase in intensity in the energy range of 2288–2306 eV resulted in the loss of these features. After exposing the oxidized sample to air for 12 weeks, a decrease in the intensity around 2296 eV caused the peak and valley to reappear, suggesting that the oxidized surface was transformed into metallic Au.

The CA of a water droplet on the untreated Au surface was 99.6° (Fig. 3(i-1), whereas a slightly lower CA of 91.7° was

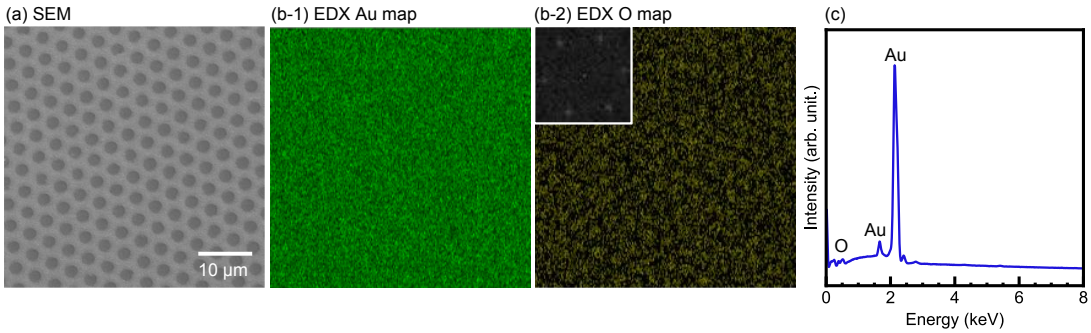

Fig. 4 SEM/EDX analysis of Au surface treated by the solid-state electrolysis using the dry PEM stamp containing a 2 μm hcp columnar pattern. (a) SEM image of Au surface. (b) EDX elemental maps of (b-1) Au and (b-2) O. The inset in (b-1) shows the corresponding 2D Fourier transform image. (c) EDX spectrum.

obtained for the Au surface after solid-state oxidation (Fig. 3(i-2)). However, a CA of 97.3° was recovered after post-oxidation air exposure for 2 months (Fig. 3(i-3)). The changes in the CA were attributed to changes in the chemical state of the Au surface. An oxidized metal surface generally shows a lower CA because of the presence of oxygen atoms, which have an affinity for water. After exposure to air for several months, the oxidized surface was reduced to metallic Au. Consequently, the CA of this surface was larger than that of the as-oxidized sample.

Several studies have investigated the electrochemical oxidation of Au surfaces to form Au_2O_3 or $Au(OH)_3$ thin film[20,21,40]. In these approaches, the use of a liquid electrolyte was essential for electrolysis. In contrast, X-ray analysis clearly demonstrated that our PEM-based solid-state electrochemical treatment can effectively oxidize Au surfaces without the use of a liquid electrolyte, thereby avoiding the necessity of waste liquid treatment.

3.3 Structure of pattered Au surfaces

The patterned Au surface formed using a dry PEM stamp with a 2 μm micropillar structure during electrolysis was observed using SEM and EDX elemental analysis. The SEM image (Fig. 4(a)) showed the formation of clear dark spots with an hcp structure on the treated Au surface. As shown in Fig. 4(b-1), EDX elemental mapping of Au revealed a uniform distribution without an hcp patterned structure. Despite the oxygen peak having a low intensity in the EDX spectrum (Fig. 4(c)), an indistinct pattern was observed in the oxygen elemental map (Fig. 4(b-2)). Moreover, the two-dimensional (2D) Fourier transform image (inset, Fig. 4(b-2)) exhibited a clear hexagonal pattern, suggesting that oxygen was distributed in an hcp arrangement on the Au surface. The SEM/EDX analysis demonstrates that a gold oxide film can be selectively formed at the contact area between the PEM stamp and material. Thus, microscale oxide pattern formation, which is difficult using conventional electrochemical treatment methods with liquid electrolytes, was realized via solid-state electrolysis.

The Au surfaces treated via solid-state anodization using the PEM stamp with a 2 μm micropillar structure were also observed using AFM. As shown in Fig. 5(a), microscale columns with an hcp arrangement were formed on the Au surfaces treated under an electrolytic bias of 3 V, which is a positive pattern relative to that on the PEM stamp (Fig. 1(c-1)). This observation indicates that the Au surface in contact with the top of the pattern on the PEM stamp was selectively oxidized, with the resulting volume expansion causing the growth of bumps on the surface. The patterned structure formed on the Au surface exhibited structural coloration, which could be observed in photographs of the sample (inset, Fig. 5(a-1)). The diameter at the top of the columns was approximately 2 μm for surfaces treated with both the dry (Fig. 5(a-1)) and wet (Fig. 5(a-2)) PEM stamps. However, the diameter of the bottom of the columns was approximately 4 μm for the Au surface treated with the wet PEM stamp, significantly exceeding that obtained when the dry PEM stamp was used (~2 μm). Furthermore, the height of the pattern obtained using the wet PEM stamp was 2 times greater than that obtained using the dry PEM stamp. The larger dimensions of the bumps formed using the wet PEM stamp are primarily due to the difference in ion conductivity between the dry and wet PEMs. As observed in the CV profiles (Fig. 2(b)), the current density of the wet PEM was superior to that of the dry PEM because sufficient nanoscale water channels could form in the wet PEM. According to Faraday's law of electrolysis, the mass of material that reacts during electrochemical treatment is proportional to the electrolytic current passing through the electrochemical cell. Therefore, the higher current density induced by the wet PEM stamp promoted effective oxide pattern formation on the Au surface.

Under an increased electrolytic bias of 4 V, smaller patterns were formed on the Au surfaces after electrolysis (Fig. 5(b)). In particular, the pattern formed on the surface treated with the dry PEM stamp differed significantly (Fig. 5(b-1)), consisting of a doughnut-shaped structure with a very low height (~50 nm). This pattern indicated that the outer periphery of the Au surface in contact with the PEM stamp was preferentially oxidized. The lack of water channel formation within the PEM stamps resulted in low ion conductivity; however, the "thirsty" dry PEM could absorb moisture from the air. Consequently, the interfacial region between the PEM stamp and surrounding air atmosphere had a higher concentration of water channels. Thus, the ion current preferentially flowed through the outer region of the PEM stamp, leading to selective and nonuniform oxidation. The lower height of the patterns obtained at a bias of 4 V with both

 This journal is © The Royal Society of Chemistry 20xx

the dry and wet PEM stamps is believed to be due to the lower electrolytic current density, as observed in the LSV profiles (Fig. 2(a)). Furthermore, the current efficiency may be lower at a bias of 4 V than at a bias of 3 V because the electrolytic current is consumed by a side reaction, with oxygen gas evolution at the interface between the Au anode and PEM stamp becoming more significant.

$$2H_2O \rightarrow O_2 + 4H^+ + 4e^- \quad (1)$$

Overall, electrochemical oxidation using the wet PEM stamp under a bias of 3 V can effectively oxidize the Au surface to form an hcp dot pattern with a diameter and height of approximately 2 μm and 400 nm, respectively. As shown in Fig. 5(c), the pattern height increases with the electrolytic time; however, it nearly saturates at approximately 550 nm after 20 min of the electrolysis. Even with shorter processing times (1 min), a pattern height of approximately 300 nm was achieved, demonstrating the efficiency of the electrochemical process in forming patterns on the Au surface.

The time-dependent changes in the pattern structure of the oxidized Au surface were investigated. As shown in Fig. 5(d), the patterned Au surface maintained the hcp dot pattern structure. However, the cross-sectional profile shown in Fig. 5(d) clearly demonstrates that the pattern height decreased to approximately 250–300 nm after one month, which was 70% of the height of the pattern on the as-oxidized sample. The decrease in pattern height was caused by the reduction of the oxide to metallic Au after air exposure[41], which was confirmed by X-ray analysis of the oxidized Au surfaces (Fig. 3). According to Takimoto et al.[7], an LSPR tip containing Au dots with a height of approximately 60 nm could be applied to toxic gas sensors. The present patterned Au surface maintain the height of several hundred nanometres even after the reduction to the metallic Au by the air exposure for 30 days, which is much larger than that for the previously reported LSPR tip, and therefore the process can be applied for the preparation of LSPR templates.

The surface morphologies of the oxide dots formed on the Au surface were observed using AFM. The untreated Au surface had an angular morphology with a high roughness of 4.64 nm *Sa* (Fig. 6(a)). In contrast, the as-oxidized Au surface observed immediately after electrochemical treatment had a significantly lower roughness of 2.65 nm *Sa* (Fig. 6(b-1)). Unlike the sharp edges of the grains in the untreated surface, the as-oxidized surface had rounded grain edges, suggesting that the sharp edges were covered with an oxide film during solid-state electrolysis. Upon air exposure, the surface roughness increased to approximately 4 nm *Sa* (Figs. 6(b-2) and (b-3)). As demonstrated

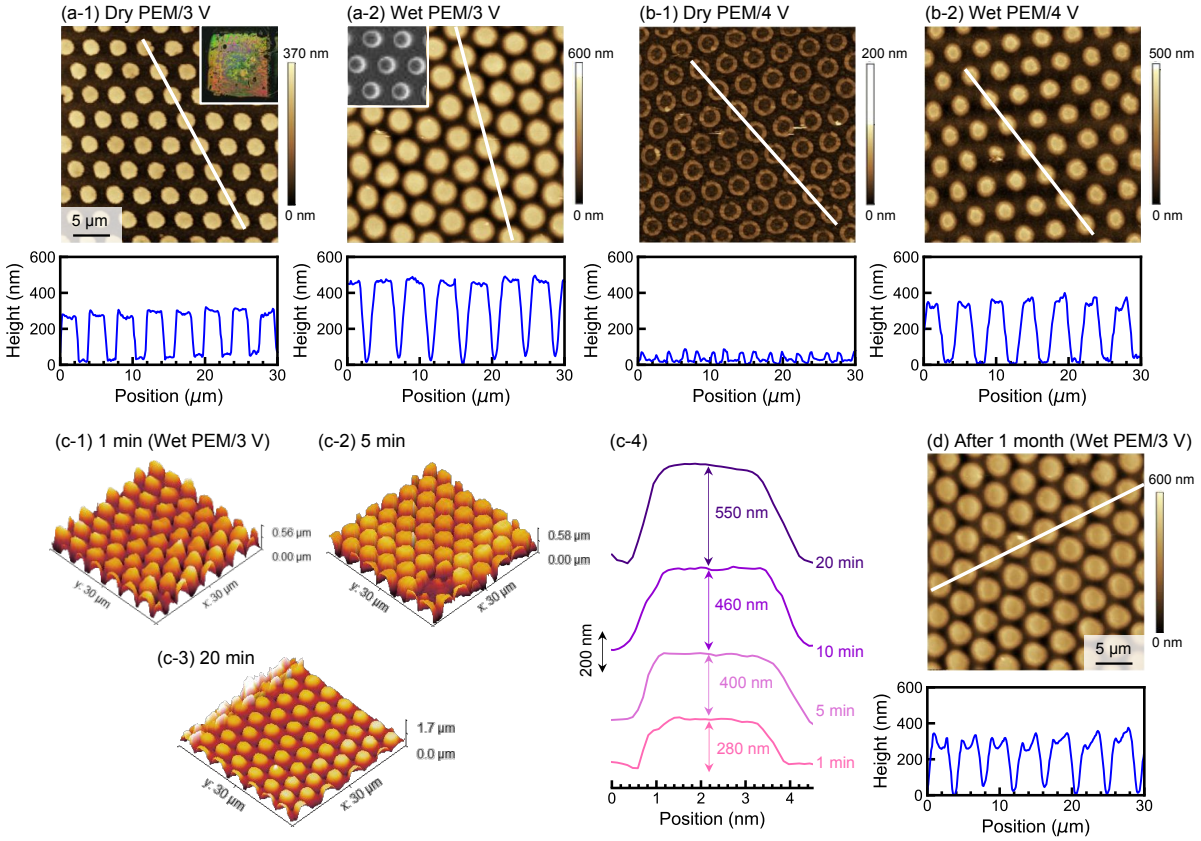

Fig. 5 (a, b) Impact of electrolytic bias and water content on the pattern structure formed on the Au surface. (Top) AFM images of Au surfaces treated using solid-state electrolysis with (1) dry and (2) wet PEM stamps containing a 2 μm hcp columnar pattern under electrolytic biases of (a) 3 and (b) 4 V for 10 min. (Bottom) Cross-sectional profiles along the lines in the AFM images. The insets in the AFM images in (a-1) and (a-2) show a photograph of the sample, which reveals the structural coloration, and an SEM image of the PEM stamp, respectively. (c) Effect of processing time on the pattern structure using the wet PEM stamp under 3 V. AFM images of Au surfaces with different processing times: (c-1) 1 min, (c-2) 5 min, and (c-3) 20 min. (c-4) Cross-sectional profile of the single pillar formed on Au surfaces with different times. (d) AFM observation of the patterned Au surface after air exposure for 4 weeks.

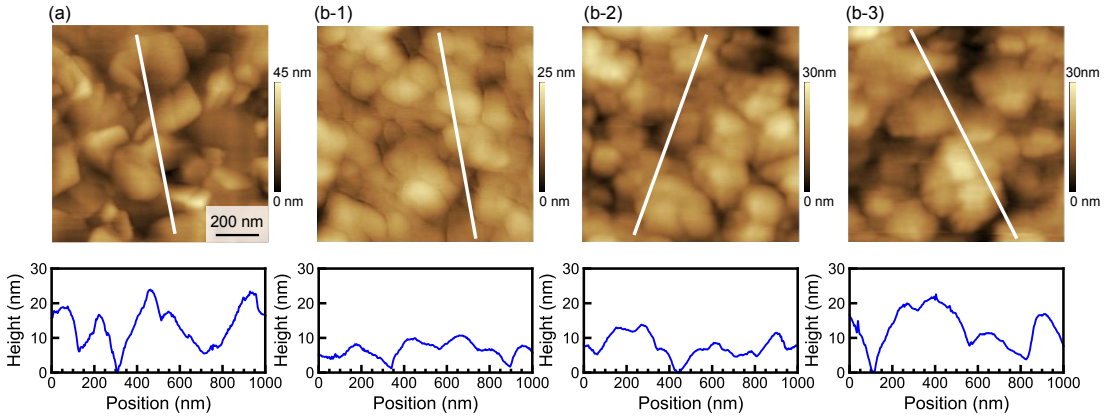

Fig. 6 (Top) Time-dependent changes in the morphology of the oxidized Au surface observed using AFM with a scan area of 1 × 1 μm^2. AFM images of (a) the untreated Au surface (roughness: 4.64 nm *Sa*) and (b) oxidized Au surfaces, in which the top of a dot was observed: (b-1) as-oxidized surface (2.65 nm *Sa*) and surfaces after air exposure for (b-2) 1 week (3.94 nm *Sa*) and (b-3) 2 weeks (4.02 nm *Sa*). (Bottom) Cross-sectional profiles along the lines in the AFM images.

by the cross-sectional profile in Fig. 6(b-3) the oxidized sample exposed to air for 2 weeks had a rough surface with a maximum height variation of approximately 20 nm. The changes in the roughness and morphology over time can be attributed to the reduction of the oxide upon exposure to the air atmosphere.

The feasibility of forming diverse patterns on Au surfaces was examined. The AFM images in Fig. 7 show gold oxide patterns formed by solid-state electrolysis using PEM stamps with line and space (L&S; Fig. 7(a-1)) or hcp hole (Fig. 7(a-2)) structures with a resolution of 2 μm. The corresponding cross-sectional profiles indicate that the pattern height varied in the range of 100–200 nm, depending on the pattern structure, likely due to differences in the real contact area between the PEM stamp and Au surfaces. Compared with the morphologies of the PEM stamps (inset, Fig. 7(a)), the oxides formed on the Au surfaces had similar pattern pitches. For open-air patterns such as the L&S (Fig. 7(a-1)) and hcp dot (Fig. 5(a-2)) structures, the lateral dimensions of the formed oxide patterns, such as the line width and dot diameter, were nearly equivalent to those of the PEM stamps. However, for the closed pattern, that is, the hcp hole structure (Fig. 7(a-2), as well as exhibiting a decreased pattern height (~100 nm), the width of the pattern was smaller than that of the PEM stamp. This phenomenon is probably due to insufficient water being supplied to the PEM stamp for the closed-pattern structure. Furthermore, as shown in Fig. 7(a-2), hexagonal holes were observed on the Au surface patterned with the hcp hole structure, indicating that the plateau of the PEM stamp was not flat.

Patterns with smaller structures were formed on Au surfaces when PEM stamps with a resolution of 500 nm were used. As shown in Fig. 7(b), submicrometric-scale L&S (Fig. 7(b-1)) and hcp hole (Fig. 7(b-2)) patterns with heights of approximately 50 nm were achieved. In the L&S pattern, the widths of the lines and spaces were 0.8 and 0.2 μm, respectively (cross-sectional profile, Fig. 7(b-1)). Thus, the increase in the oxide pattern dimensions caused by volume expansion was more significant during submicrometric resolution patterning. These results demonstrate that diverse patterned structures with resolutions in the range of several micrometres to several hundred nanometres can be formed via solid-state electrochemical oxidation.

Further insights into the structures of the patterned Au surfaces were obtained by immersing the samples in 0.1 mol/L

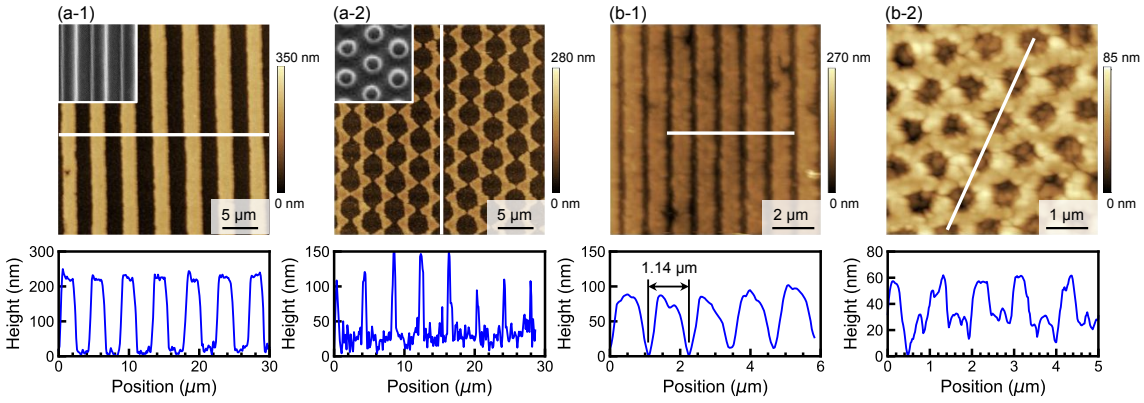

Fig. 7 (Top) AFM images of patterned Au surfaces with different structures and resolutions: (a-1) L&S (2 μm), (a-2) holes (2 μm), (b-1) L&S (500 nm), and (b-2) holes (500 nm). The insets in (a-1) and (a-2) show SEM images of the PEM stamps used for electrolysis. (Bottom) Cross-sectional profiles along the lines in the AFM images.

This journal is © The Royal Society of Chemistry 20xx

Please do not adjust margins

KOH aqueous solution and monitoring changes in the surface morphology using AFM with a scan area of 10 × 10 μm^2. As shown in Fig. 8(a-1), the as-oxidized surface exhibited an hcp dot pattern with a height and diameter of approximately 200 nm and 2 μm, respectively. After immersion in the KOH solution for 15 min, the pattern height decreased significantly to less than 50 nm (Fig. 8(a-2)). Wet KOH treatment for 30 min almost completely removed the pattern and formed a smooth Au surface (Fig. 8(a-3)). However, further increasing the immersion time in the KOH solution resulted in a negative and dimpled pattern on the Au surface (Figs. 8(a-4) and (a-5)). After immersion for 120 min, the formed dimples had a depth of approximately 70 nm. These results suggest that the gold oxide formed by electrolysis could be removed in alkaline solution and that the oxide film grew not only on the surface but also in the subsurface region. Similar oxide film growth mechanisms have been observed for Si[28] and Ti[24] surfaces treated via solid-state electrochemical oxidation.

As shown by the OM image after KOH treatment for 120 min (Fig. 8(b-2)), along with the formation of a dimpled morphology, flaky and particulate matter was generated and aggregated in certain regions of the Au surface. These particles are believed to "cap" the Au surface and be detached by the wet KOH treatment. Compared with the oxide dots formed on the as-oxidized surface (Fig. 8(b-1)), the diameters of the caps decrease to 0.5–1 μm after KOH treatment, which indicates that the cap particles dissolved slightly in the KOH solution. The detachment of these caps from the Au surface suggests that the oxidized region neighbouring the oxide–bulk Au interface is more soluble in the KOH solution than the topmost surface of the oxide, leading to preferential removal by the alkaline etchant, as illustrated in Fig. 8(c). The top region of the oxidized layer, which was more difficult to etch, was subsequently removed from the sample in particulate form. According to previous reports[42,43], Au_2O_3 readily dissolves in alkaline solution, whereas $Au(OH)_3$ exhibits poor solubility in aqueous solution. As the wet KOH treatment was conducted at room temperature (~22 °C), the modified layer may have comprised a double layer, in which a $Au(OH)_3$ film forms on the underlying Au_2O_3 layer present at the interface with bulk Au (Fig. 8(c)). As discussed previously, the electrochemically formed oxide film was unstable and underwent reduction in air. After forming the Au_2O_3 layer via solid-state electrolysis, the top surface preferentially reacted with moisture in the atmosphere to form $Au(OH)_3$. However, the underlying Au_2O_3 oxide layer was protected from air exposure and thus maintained its initial chemical composition.

3.4 Optical properties of oxidized Au surfaces

The optical properties of the oxidized Au surfaces were investigated by monitoring time-dependent changes in the reflectance of the Au surface treated with the nonpatterned PEM. The untreated Au surface exhibited a reflectance of approximately 50% at wavelengths of 400–500 nm, but the reflectance drastically increased to more than 90% at wavelengths greater than 550 nm (Fig. 9(a)). For the as-oxidized Au surface, the reflectance was lower over the entire wavelength range. Moreover, exposure to air for 1 month at room temperature (~22 °C) further decreased the reflectance at

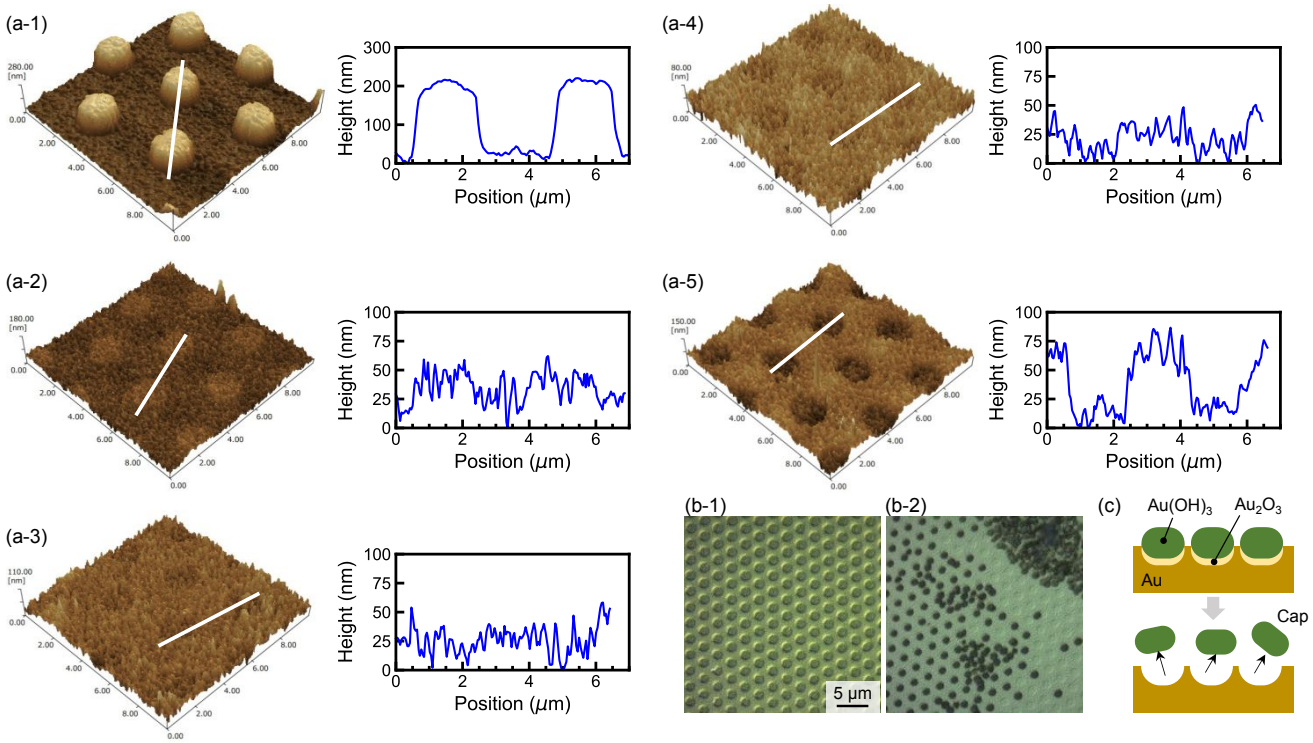

Fig. 8 Evolution of the surface pattern structure during wet KOH immersion. (Left) (a) AFM images of the (a-1) as-oxidized surface and surfaces treated with KOH for (a-2) 15, (a-3) 30, (a-4) 60, and (a-5) 120 min. (Right) Cross-sectional profiles along the lines in the AFM images. (b) OM images of the (b-1) as-oxidized surface and (b-2) surface after KOH immersion for 120 min. (c) Schematic of the double-layered oxide formed on the Au surface.

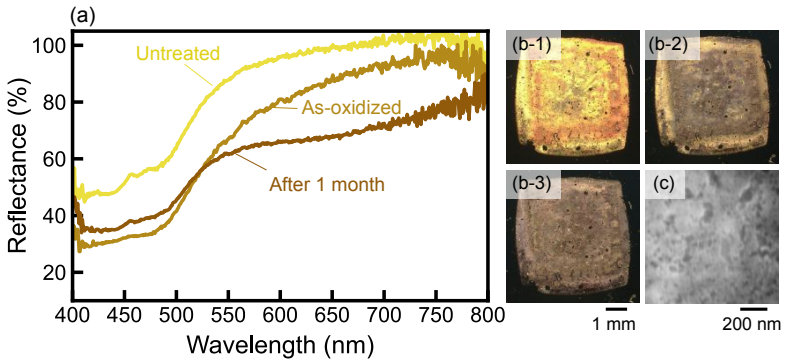

Fig. 9 (a) Reflectance spectra of pristine Au surface and oxidized Au surfaces treated with the nonpatterned PEM. (b) OM images of oxidized Au samples: (b-1) as-oxidized surface and surfaces after air exposure for (b-2) 1 week and (b-3) 1 month. (c) SEM image of the oxidized Au surface after air exposure for 1 month.

wavelengths greater than 520 nm. This decrease in the reflectance can be observed in the corresponding photographs of the samples (Fig. 9(b)). A similar decrease in reflectance was reported by Nishio et al.[20] for gold oxide films formed using liquid-based electrochemical anodization in a citric acid aqueous solution. XPS and electron microscopy analyses of the anodized surface demonstrated that the gold oxide film was gradually reduced to metallic Au over time, with a black unoxidized Au film with a nanoporous structure forming on the treated surface. A highly porous surface can effectively absorb incident light, resulting in a lower reflectance. Because of the high antioxidant properties of noble metals, the gold oxide film was unstable in air and thus easily reduced to form an unoxidized metallic layer. The high-magnification SEM image of the oxidized Au surface after 30 days (Fig. 9(c)) reveals the formation of a porous structure on the treated area.

Angle-resolved reflectance spectra were measured to investigate the structural coloration observed on the Au surface patterned using the 500 nm L&S PEM stamp (Fig. 10(a-1)). As shown by the reflectance spectra at different collection angles θ_m in the range of 5°–25° (Fig. 10(b)), the L&S pattern with 500 nm resolution exhibited reflective diffraction grating characteristics. In particular, the position of the sharp reflectance peak was strongly dependent on the measurement angle. According to the grating equation[44], the relationship between the diffraction angle and wavelength for a reflective diffraction grating can be expressed as follows:

$$d\,(\sin\theta_i - \sin\theta_m) = m\lambda \qquad (2)$$

where d is groove spacing, θ_m is the diffraction angle for order m, θ_i is the incident angle, and λ is the wavelength (Fig. 10(a-2)). At a fixed incident angle θ_i of 60°, groove spacing d can be determined from the θ_m and λ values extracted from the reflectance spectra in Fig. 10(a). However, each refraction spectrum exhibited two peaks. Thus, the peaks with higher and lower intensities were defined as the primary (wavelength of λ_p) and satellite peaks (λ_{sat}), respectively. The groove spacings for

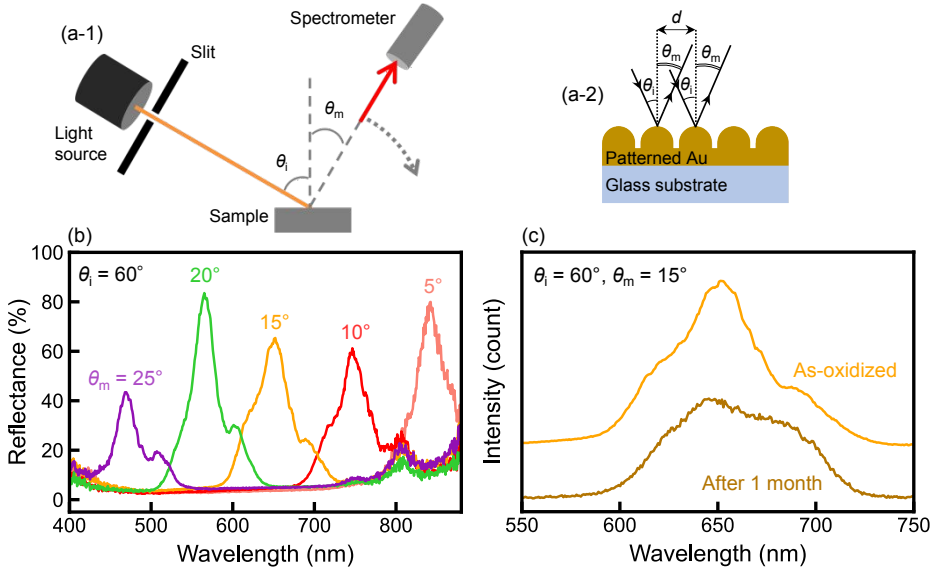

Fig. 10 Angle-resolved reflectance spectra of the patterned Au surface treated with the 0.5 μm L&S PEM stamp. The incident angle of the halogen lamp illumination source was 60°. (a) Schematic illustration of (a-1) measurement setup and (a-2) reflective grating. (b) Reflectance of the as-patterned Au surface at various collection angles. (c) Comparison of the reflectance intensities of the patterned Au surface before and after air exposure for 4 weeks. The collection angle was 15°.

This journal is © The Royal Society of Chemistry 20xx

Please do not adjust margins

the primary and satellite peaks, calculated using the grating equation, are listed in Table 1.

Table 1 Relationship between diffraction angle θ_m, peak wavelength λ of diffracted light, and groove spacing d. The incident angle θ_i was fixed at 60°.

θ_m (°)	λ_p (nm)*1	d_p (μm)*2	λ_{sat} (nm)*1	d_{sat} (μm)*2
5	844	1.08	-	-
10	747	1.08	-	-
15	654	1.08	693	1.14
20	568	1.08	611	1.17
25	471	1.06	511	1.15

*1 The peak wavelengths of the diffracted light were extracted from the reflectance spectra in Fig. 10(a).
*2 Groove spacing d was estimated using the grating equation (Eq. (2)) with order m of 1:

The average groove spacing for the primary peak (d_p) was calculated to be 1.08 μm, which is slightly smaller than the actual groove spacing determined from the AFM cross-sectional profile of the patterned Au surface (Fig. 7(b-1)). However, for the satellite peak, the average groove spacing (d_{sat}) was calculated to be 1.15 μm, which agrees well with the actual groove spacing of approximately 1.14 μm obtained from AFM observations. Therefore, the satellite peaks in the reflectance spectra may originate from the interference of light diffracted by the grooves on the Au surface. The larger groove spacing of the primary peak (d_p) may be due to the geometry of the oxide pattern formed on the Au surface or differences in the refractive indices of the gold oxide and metallic Au. Reflectance spectra with multiple peaks have also been reported by Aoyama et al.[45] for a template consisting of Au nanoparticles on a Au thin film coated on a glass substrate via a phenomenon called Fano resonance. Lei et al.[46] reported that a particle-on-film structure consisting of Au nanospheres on a Au thin film exhibits a scattering spectrum with multiple peaks that originate from interactions between the nanospheres and the thin film deposited on a glass substrate. The patterned Au surface prepared by solid-state electrochemistry had a similar three-layered structure, consisting of a nanopatterned film on a Au thin film over a glass substrate. Thus, the double peaks in the reflectance spectra are believed to be derived from interactions between the nanostructures and Au thin film in the multilayer structure.

Fig. 10(b) shows the reflectance spectrum of the patterned Au sample collected at a measurement angle θ of 15° after air exposure for 1 month. Compared with the spectrum of the as-oxidized sample immediately after patterning, the reflection intensity was decreased. However, even after air exposure for 1 month, the patterned Au surface retained reflective diffraction grating characteristics. As revealed by XPS analysis of the treated Au surfaces (Fig. 3), the oxide layer formed on the Au surface was almost completely reduced to metallic Au after air exposure for 2 weeks. However, AFM imaging (Fig. 5(c)) showed that patterned structures were maintained even after 1 month. Thus, structural coloration was still observed on the L&S-patterned Au surface despite none of the anodic oxide film remaining on the surface.

4. Conclusion

A novel, fast, and facile patterning method using solid-state electrochemical oxidation with PEM stamps was applied to Au surfaces. Electrochemical measurements showed that the wet PEM achieved a higher oxidation current than the dry PEM. XPS analysis of the chemical composition confirmed the presence of Au^{3+} peaks, associated with Au_2O_3 or $Au(OH)_3$, on the oxidized Au surface, whereas the untreated surface only exhibited metallic Au peaks. After the treated sample was exposed to air for 2 weeks, the intensity of the Au^{3+} peaks decreased significantly, indicating that the oxide film was reduced to form metallic Au. Under an electrolytic voltage of 3 V, the formation of microscale oxide patterned structures via electrochemical imprinting was more efficient with the wet PEM stamp than with the dry PEM. A higher electrolytic voltage resulted in a nonuniform pattern with a smaller height. Although reduction of the oxide via air exposure decreased the height of the patterned structure by approximately 70% relative to that of the as-oxidized sample, the surface still maintained a pattern height of several hundred nanometres. However, the microroughness at the top of the pattern increased over time. Oxide patterns containing L&S, hole, and dot structures with micrometric (2 μm) and submicrometric (500 nm) resolutions were successfully formed on Au surfaces via electrolysis for 10 min. The oxide dot pattern was removed after immersion in KOH solution to form a dimpled pattern with a depth of ~50 nm, and OM observations suggested that the oxide film had a multilayer structure, in which a top insoluble layer covered an underlying readily soluble layer. The angle-resolved reflectance spectra of the L&S-patterned Au surface with a resolution of 500 nm exhibited high-intensity sharp peaks that depended on the measurement angle. Although further investigation of the patterning characteristics, such as the PEM stamp lifetime and pattern resolution limit, is required, the present imprinting method based on solid-state electrochemical oxidation is promising for the fast and facile preparation of micro- and nanoscale Au patterns with potential applicability as optical gratings and LSPR templates for bio/chemical sensors.

Author contribution

J. M. conceived the study. T. F. and A. T. designed and conducted the experiments. M. T. performed the X-ray analyses. J. M. and T. F. co-authored the manuscript. J. M., K. Y., and A. T. discussed and analysed the data. All authors read and approved the final manuscript.

Conflicts of interest

There are no conflicts to declare

Acknowledgements

This research was partially supported by grants from the JST FOREST Program (Grant Number JPMJFR222P) and JSPS KAKENHI (Grant Numbers 23K17725 and 23H01320).

References

1 M. Sankar, Q. He, R. V. Engel, M. A. Sainna, A. J. Logsdail, A. Roldan, D. J. Willock, N. Agarwal, C. J. Kiely and G. J. Hutchings, Chem. Rev., 2020, 120, 3890–3938.
2 Y. Bing, H. Liu, L. Zhang, D. Ghosh and J. Zhang, Chem. Soc. Rev., 2010, 39, 2184–2202.
3 P. Si, N. Razmi, O. Nur, S. Solanki, C. M. Pandey, R. K. Gupta, B. D. Malhotra, M. Willander and A. De La Zerda, Nanoscale Adv., 2021, 3, 2679–2698.
4 Y. Singh, M. K. Paswan and S. K. Raghuwanshi, Plasmonics, 2021, 16, 1781–1790.
5 T. Tokoroyama, M. Murashima and N. Umehara, Tribol. Online, 2020, 15, 300–308.
6 A. Monkawa, T. Nakagawa, H. Sugimori, E. Kazawa, K. Sibamoto, T. Takei and M. Haruta, Sensors Actuators, B Chem., 2014, 196, 1–9.
7 Y. Takimoto, A. Monkawa, K. Nagata, M. Kobayashi, M. Kinoshita, T. Gessei, T. Mori and H. Kagi, Plasmonics, 2020, 15, 805–811.
8 D. Panjwani, M. Yesiltas, J. Nath, D. E. Maukonen, I. Rezadad, E. M. Smith, R. E. Peale, C. Hirschmugl, J. Sedlmair, R. Wehlitz, M. Unger and G. Boreman, Infrared Phys. Technol., 2014, 62, 94–99.
9 T. Xia, H. Luo, S. Wang, J. Liu, G. Yu and R. Wang, Cryst. Eng. Comm., 2015, 17, 4200–4204.
10 M. T. Do, Q. C. Tong, A. Lidiak, M. H. Luong, I. Ledoux-Rak and N. D. Lai, Appl. Phys. A Mater. Sci. Process., 2016, 122, 1–6.
11 N. G. Quilis, S. Hageneder, S. Fossati, S. K. Auer, P. Venugopalan, A. Bozdogan, C. Petri, A. Moreno-Cencerrado, J. L. Toca-Herrera, U. Jonas and J. Dostalek, J. Phys. Chem. C, 2020, 124, 3297–3305.
12 S. Y. Chou, P. R. Krauss and P. J. Renstrom, J. Vac. Sci. Technol. B Microelectron. Nanom. Struct. Process. Meas. Phenom., 1996, 14, 4129–4133.
13 S. H. Kwak, J. S. Wi, J. Lee, C. Kim and H. K. Na, RSC Adv., 2022, 12, 15652–15657.
14 W. I. Park, T. W. Park, Y. J. Choi, S. Lee, S. Ryu, X. Liang and Y. S. Jung, ACS Nano, 2021, 15, 10464–10471.
15 T. Lednický and A. Bonyár, ACS Appl. Mater. Interfaces, 2020, 12, 4804–4814.
16 Y. Brasse, V. Gupta, H. C. T. Schollbach, M. Karg, T. A. F. König and A. Fery, Adv. Mater. Interfaces, 2020, 7, 201901678.
17 E. S. A. Goerlitzer, M. Zhan, S. Choi and N. Vogel, Langmuir, 2023, 39, 5222–5229.
18 M. Rahaman, S. Moras, L. He, T. I. Madeira and D. R. T. Zahn, J. Appl. Phys., 2020, 128, 233104.
19 F. Bonaccorso, G. Calogero, G. Di Marco, O. M. Maragò, P. G. Gucciardi, U. Glorgianni, K. Channon and G. Sabatino, Rev. Sci. Instrum., 2007, 78, 103702.
20 K. Nishio and H. Masuda, Bull. Chem. Soc. Jpn., 2013, 86, 1144–1150.
21 K. Nishio and H. Masuda, Angew. Chemie - Int. Ed., 2011, 50, 1603–1607.
22 R. Umezaki and J. Murata, Mater. Chem. Phys., 2021, 259, 124081.
23 S. Zulkifle, K. Hayama and J. Murata, Diam. Relat. Mater., 2021, 120, 108700.
24 P. Jia, R. Umezaki and J. Murata, Microelectron. Eng., 2022, 257, 111752.
25 J. Murata, K. Hayama and M. Takizawa, Appl. Surf. Sci., 2023, 625, 157190.
26 A. Tsuji, E. Morimoto, M. Takizawa and J. Murata, Adv. Mater. Interfaces, 2024, 11, 2300896.
27 J. Murata, Y. Nishiguchi and T. Iwasaki, Electrochem. commun., 2018, 97, 110–113.
28 K. Yamazaki, A. Tsuji, M. Takizawa and J. Murata, Small Methods, 2024, 2301787, 1–11.
29 K. Talukdar, P. Gazdzicki and K. A. Friedrich, J. Power Sources, 2019, 439, 227078.
30 M. Todeschini, A. Bastos Da Silva Fanta, F. Jensen, J. B. Wagner and A. Han, ACS Appl. Mater. Interfaces, 2017, 9, 37374–37385.
31 R. Yadav and P. S. Fedkiw, J. Electrochem. Soc., 2012, 159, B340–B346.
32 B. Qian, P. Sultana, P.-J. Chen, G. Mensing and P. Ferreira, J. Manuf. Process., 2022, 79, 305–313.
33 C. Feng and P. F. He, RSC Adv., 2017, 7, 34556–34566.
34 T. Li, J. Shen, G. Chen, S. Guo and G. Xie, ACS Omega, 2020, 5, 17628–17636.
35 A. R. Silva Olaya, B. Zandersons and G. Wittstock, Chem. Electro. Chem., 2020, 7, 3670–3678.
36 K. Juodkazis, J. Juodkazyte, V. Jasulaitiene, A. Lukinskas and B. Šebeka, Electrochem. commun., 2000, 2, 503–507.
37 P. Hepperle, A. Herman, B. Khanbabaee, W. Y. Baek, H. Nettelbeck and H. Rabus, Part. Part. Syst. Charact.
38 M. Peuckert, F. P. Coenen and H. P. Bonzel, Surf. Sci., 1984, 141, 515–532.
39 M. Pourbaix and J. A. Franklin, Atlas of electrochemical equilibria in aqueous solutions, National Association of Corrosion Engineers, 1974.
40 D. H. Nagaraju and V. Lakshminarayanan, J. Phys. Chem. C, 2009, 113, 14922–14926.
41 H. Tsai, E. Hu, K. Perng, M. Chen, J. C. Wu and Y. S. Chang, Surf. Sci., 2003, 537, L447–L450.
42 M. Higo, K. Ono, K. Yamaguchi, M. Mitsushio, T. Yosmdome and S. Nakatake, Anal. Sci., 2020, 36, 1081–1089.
43 D. Kawamoto, H. Ando, H. Ohashi, Y. Kobayashi, T. Honma, T. Ishida, M. Tokunaga, Y. Okaue, S. Utsunomiya and T. Yokoyama, Bull. Chem. Soc. Jpn., 2016, 89, 1385–1390.
44 R. D. Boyd, J. A. Britten, D. E. Decker, B. W. Shore, B. C. Stuart, M. D. Perry and L. Li, Appl. Opt., 1995, 34, 1697.
45 Y. Aoyama, A. Toyotama, T. Okuzono, N. Hirashima, H. Imai, F. Uchida, Y. Takiguchi and J. Yamanaka, Chem. Pharm. Bull., 2022, 70, 130–137.
46 D. Y. Lei, A. I. Fernández-Domínguez, Y. Sonnefraud, K. Appavoo, R. F. Haglund, J. B. Pendry and S. A. Maier, ACS Nano, 2012, 6, 1380–1386.

This journal is © The Royal Society of Chemistry 20xx

The data supporting this article have been included as part of the Supplementary Information.